Material parameter identification from full-field data in the context of linear elasticity

Narunat Pantapalin [1] (✉)

Abstract This report focuses on identifying material parameters for linear elastic materials using full-field data and finite element simulations. The report involves dataset preparation, forward problem formulation, and simulations employing the Finite Element Method (FEM) implemented in FEniCSx. The goal is to calibrate shear modulus (G) and bulk modulus (K) through supervised regression techniques by minimizing loss functions comparing numerical and experimental displacement data. A reduced identification problem is formulated using state and observation equations, with numerical solutions (FEM) derived for the linear elasticity problem under specified boundary conditions. The optimization, using the L-BFGS-B algorithm, yields calibrated material parameters: G and K, with relative deviations from prior studies. The results include displacement fields and error analysis, providing insights into regions contributing to discrepancies.

Keywords Material Parameter Identification from full-field data, FEM, FeniCSx

1 Introduction

Supervised regression/identification of material parameters

$$\boldsymbol{\kappa}^* = \arg\min_{\boldsymbol{\kappa}} \left|\left| \mathbf{P}_i - \frac{\partial W(\mathbf{F};\boldsymbol{\kappa})}{\partial \mathbf{F}} \right|\right|_{\bullet}^2 \tag{1}$$

Depending on wheter $\mathbf{P}$ is provided as vector (Voigt Notation) or second order tensor, $\bullet$ or Frobenius norm.

The course advanced data-driven modeling covers reduced and all-at-once approaches in solid me chanics, see also Römer et al. [2024]. We will discover physics-informed neural networks in an all-at-once, as well as in a reduced setting, see Anton and Wessels [2022] and Anton et al. [2024]. Moreover, we will discover reduced approaches with parametric surrogates, see Paul et al. [2024] and Agarwal et al. [2024].

(1) Division Data-driven modeling of mechanical systems, Technische Universtität Braunschweig, Pockelsstraße 3, 38106 Braunschweig E-mail: h.wessels@tu-braunschweig.de

2 Identification from full-field data

The identification problem is described by two equations:

$$\begin{aligned} \mathbf{F}(\mathbf{y};\boldsymbol{\kappa}) &= \mathbf{0} \quad \text{(state equation)} \\ \mathbf{O}(\mathbf{y}) &= \mathbf{d} \quad \text{(observation equation)} \end{aligned} \tag{2}$$

Assume that $\mathbf{y}(\boldsymbol{\kappa})$ (implicit function theorem). Then, Parameters are identified from:

$$\boldsymbol{\kappa}^* = \arg\min_{\boldsymbol{\kappa}} ||\mathbf{O}(y) - d||_2^2 \tag{3}$$

which is referred to as the reduced identification problem in Römer et al. [2024]. The solution of $\mathbf{y}(\boldsymbol{\kappa})$ under consideration of the state equation is discussed in Section 3

- The observation operator $\mathbf{O}$ only selects the nodes/discretization points that contribute to the loss. Thus, it does neither depend on the state nor on the material parameters and we do not need to differentiate it during optimization.
- The data $\mathbf{d}$ is interpolated from the sensor locations to the numerical discretization, where we refer to it as $\tilde{\mathbf{d}}$. This interpolation needs to be carried out once prior to the optimization.

With these modifications, the parameter identification problem writes:

$$\begin{aligned} \boldsymbol{\kappa}^* &= \arg\min_{\boldsymbol{\kappa}} \left|\left|\mathbf{O}(y) - \tilde{\mathbf{O}}(d)\right|\right|_2^2 \\ &= \arg\min_{\boldsymbol{\kappa}} \left|\left|\mathbf{O}(y) - \tilde{\mathbf{d}}\right|\right|_2^2 \\ &= \arg\min_{\boldsymbol{\kappa}} \mathcal{L}(\mathbf{y}(\boldsymbol{\kappa})) \end{aligned} \tag{4}$$

- Defined the methods for numerical solution of $\mathbf{y}(\boldsymbol{\kappa})$: see Section 3
- The interpolation of sensor data onto discretization nodes: see Section 4
- The differentiation of loss function using automatic differentiation

3 Forward Problem

3.1 Fundamental Theory

To identify the material parameters of a specimen, we consider a forward problem involving small elastic deformations, which are governed by the balance of linear momentum:

$$\rho_0 \mathbf{a} = \boldsymbol{\nabla}\cdot\mathbf{P} + \rho_0 \mathbf{b} \tag{5}$$

where ρ_0 represents the initial density, $\mathbf{a}$ denotes the acceleration, $\mathbf{P}$ is the first Piola-Kirchhoff stress tensor (a second-order tensor), and $\mathbf{b}$ corresponds to the acceleration due to body forces, such as gravity. With constitutive equation (Linear Elasticity).
Dirichlet and Neumann boundary conditions are defined as:

$$\begin{aligned} \mathbf{u} &= \bar{\mathbf{u}} \text{ on } \Gamma_D \\ \mathbf{P}\cdot\mathbf{N} &= \bar{\mathbf{T}} \text{ on } \Gamma_N \end{aligned} \tag{6}$$

For linear, isotropic elasticity and small strains, the constitutive model states.

$$\begin{aligned} \mathbf{P} &= \frac{\partial W(\mathbf{F};\boldsymbol{\kappa})}{\partial \mathbf{F}} \\ \mathbf{P} &= K\ \mathrm{tr}(\boldsymbol{\epsilon}(\mathbf{u}))\mathbf{I} + 2G(\boldsymbol{\epsilon}(\mathbf{u}) - \frac{\mathrm{tr}(\boldsymbol{\epsilon}(\mathbf{u}))}{3}\mathbf{I}) \end{aligned} \tag{7}$$

Herein, K and G represents bulk modulus and shear modulus respectively and become the parameters for identification $\boldsymbol{\kappa} = \{G, K\}^T$. The linear strain $\boldsymbol{\epsilon}$ is defined as

$$\boldsymbol{\epsilon}(\mathbf{u}) = \frac{1}{2}(\boldsymbol{\nabla}\mathbf{u}(\mathbf{X}) + (\boldsymbol{\nabla}\mathbf{u}(\mathbf{X}))^T) \tag{8}$$

which $\mathbf{u}$ is deformation vector, and $\mathbf{X}$ is the vector of coordination on the initial configuration

3.2 Numerical solution

In this simulation, the finite element method (FEM) is employed to solve the boundary value problem. Starting from Equation (5), the weak form is derived by multiplying the equation by a test function $\delta\mathbf{u} \in V$, where V is a vector-valued test function space, and integrating over the entire domain Ω with respect to $\mathrm{d}\mathbf{x}$.

$$\int_\Omega \rho_0 \mathbf{a} \cdot \delta\mathbf{u}\, dx = \int_\Omega (\boldsymbol{\nabla}\cdot\mathbf{P}) \cdot \delta\mathbf{u}\, dx + \int_\Omega \rho_0 \mathbf{b} \cdot \delta\mathbf{u}\, dx \tag{9}$$

Since the system is considered to be in a static state, $\mathbf{a} = \mathbf{0}$, and there are no accelerations caused by body-force, $\mathbf{b} = \mathbf{0}$.

$$\begin{aligned} \int_\Omega (\boldsymbol{\nabla}\cdot\mathbf{P}) \cdot \delta\mathbf{u}\, dx &= 0 \\ \int_\Omega \mathbf{P} : \nabla\delta\mathbf{u}\, dx - \int_{\Gamma_N} (\mathbf{P}\cdot\mathbf{n}) \cdot \delta\mathbf{u}\, ds &= 0 \end{aligned} \tag{10}$$

The traction at the Neumann boundary is given by $\mathbf{P}\cdot\mathbf{n} = \bar{\mathbf{T}}$. The resulting weak form, which is formulated to be minimal and suitable for implementation in FEniCSx, is to solve for $\mathbf{u}$ such that:

$$\begin{aligned} \int_\Omega \sigma(\mathbf{u}) : \nabla\delta\mathbf{u}\, dx &= \int_{\partial\Omega} \bar{\mathbf{T}} \cdot \delta\mathbf{u}\, ds \\ \boldsymbol{\sigma}(\mathbf{u}) &= K\ \mathrm{tr}(\boldsymbol{\epsilon}(\mathbf{u}))\mathbf{I} + 2G(\boldsymbol{\epsilon}(\mathbf{u}) - \frac{\mathrm{tr}(\boldsymbol{\epsilon}(\mathbf{u}))}{3}\mathbf{I}) \\ \boldsymbol{\epsilon}(\mathbf{u}) &= \frac{1}{2}(\boldsymbol{\nabla}\mathbf{u}(\mathbf{X}) + (\boldsymbol{\nabla}\mathbf{u}(\mathbf{X}))^T) \end{aligned} \tag{11}$$

The FEniCSx library (Baratta et al. [2023]) was used to solve the forward problem. The code implementation can be found in the .ipynb in the attachment folder. The numerical method discretizes the balance of linear momentum (state equation) to solve for the unknown displacements $\mathbf{y}(\mathbf{X};\boldsymbol{\kappa}) = \mathbf{u}^{FEM}(X)$.

4 Results

4.1 Simulation Setup

4.1.1 Geometry, meshing and boundary conditions

The specimen geometry, meshed using triangular elements of size 0.5×10^{-3} m, consists of 9,753 nodes and 19,100 elements. This mesh configuration is utilized for the simulation and its geometry is illustrated in the figure below.

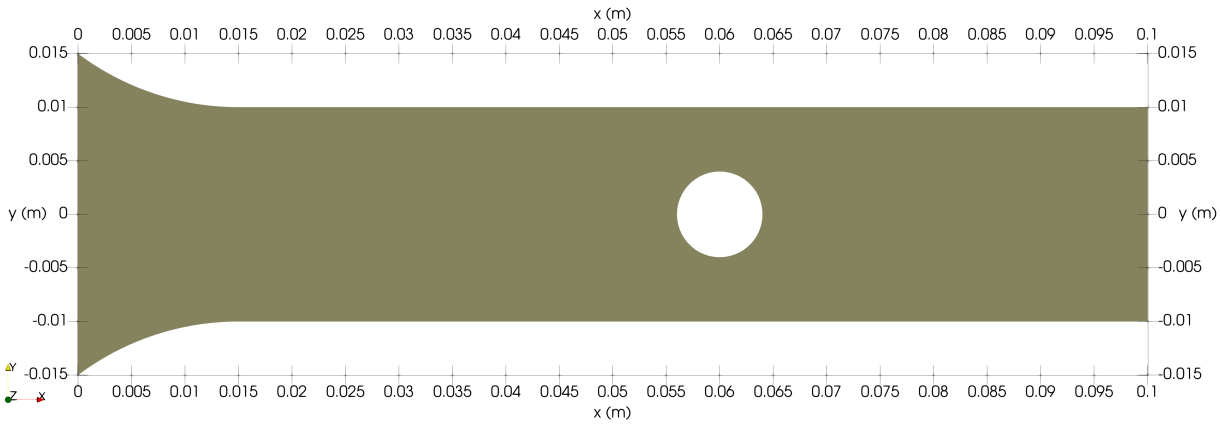

Figure 1: The geometry of the specimen and its dimension in meter.

At x = 0.0 m edge of the specimen exists a Dirichlet boundary condition (on Γ_D) with the displacement $\bar{\mathbf{u}} = \mathbf{0}$, since it is where the specimen is clamped. Secondly, the edge at x = 0.1 m consists of a Neumann boundary condition (on Γ_N) with $\bar{\mathbf{T}} = \begin{bmatrix} 106.26 & 0 \end{bmatrix}^T N/mm^2$

4.1.2 Data Collection

The experimental dataset presented in Tröger et al. [2024] is utilized for the calibration of material parameters for the specimen under investigation. To interpolate the experimental data into the finite element method (FEM) discretization, griddata function with linear interpolation is applied to map the experimental measurements onto the FEM mesh nodes. To address NaN values problem in the interpolated data, a mean neighborhood approach is implemented for filling any resulting NaN values. Figure 2 depicts the interpolated experimental data on the FEM discretization.

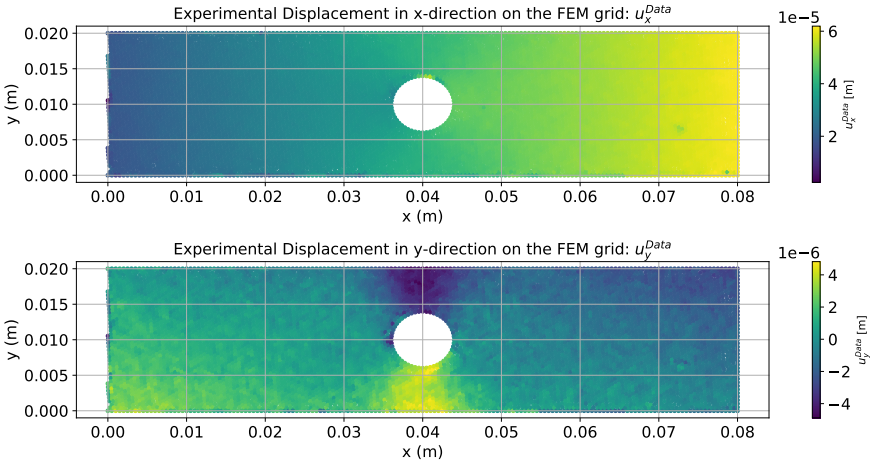

Figure 2: The interpolated experimental data on the FEM discretization.

4.1.3 Optimizer

From Equation 4, the material parameters are identified using the loss function defined inAnton et al. [2024]:

$$L(\boldsymbol{\kappa}) = \frac{1}{2}\|\mathbf{W} \cdot (O(\mathbf{u}^{FEM}(\boldsymbol{\kappa})) - \tilde{\mathbf{u}}^{Data})\|^2 \tag{12}$$

is used, where $\mathbf{u}^{FEM}$ is the solution from FEM simulation, The operator O serves as the observation operator, extracting a specific region of the solution domain to align with the experimental data region, $\tilde{\mathbf{u}}^{Data}$ is the interpolated experimental data to discretization grid of the FEM simultion. $\mathbf{W}$ denotes weights matrix consists of sub-weight matrices:

$$\mathbf{W} := \begin{bmatrix} \mathbf{W}_x & 0 \\ 0 & \mathbf{W}_y \end{bmatrix} \quad , \mathbf{W} \in \mathbb{R}^{2n_d \times 2n_d} \tag{13}$$

$$\begin{aligned} \mathbf{W}_x &= \frac{1}{u_x^{mean}}\mathbf{I} \\ \mathbf{W}_y &= \frac{1}{u_y^{mean}}\mathbf{I} \end{aligned} \tag{14}$$

with the identity matrix $\mathbf{I}$ of size $n_d \times n_d$, where u_x^{mean}, u_y^{mean} are the mean absolute of the interpolated experimental displacement in x and y respectively and defined as:

$$\begin{aligned} u_x^{mean} &= \frac{1}{n_d}\sum_{i=0}^{n_d} |u_x^{(i)}| \\ u_y^{mean} &= \frac{1}{n_d}\sum_{i=0}^{n_d} |u_y^{(i)}| \end{aligned} \tag{15}$$

The algorithm L-BFGS-B with initial guess of shear modulus $G = 10^9$ Pa and bulk modulus $K = 10^9$ Pa was used. At the end, the optimization took 29 iterations, 132 function evaluations and 44 Jacobian evaluations to complete.

4.2 Result

The result of the parameter identification is 72.24 GPa for Shear Modulus (G) and 91.69 GPa for Bulk Modulus (K) which relatively deviate from Anton et al. [2024] which are 73.541 GPa for Shear Modulus and 128.085 GPa for Bulk Modulus by $RD_G = 1.55\%$ and $RD_K = 28.22\%$. Figure 3 depicts the displacement fields in the x-direction and y-direction in meters. The Figure 4 shows the absolute errors in the x-direction (AE_x) and y-direction (AE_y) in meters which calculate the difference between $\mathbf{u}_i^{FEM}$ and $O(\mathbf{u}^{Data})_i$ where i is the node of the discretized domain. Both AE_x and AE_x are high near critical regions of the geometry, such as around the hole and along the left edge (Figure 4).

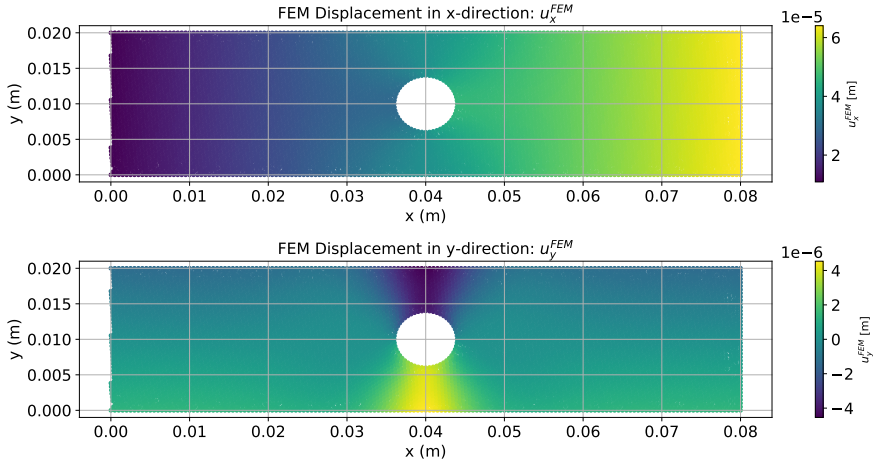

Figure 3: Displacement fields in x- and y-direction from FEM simulation with the calibrated bulk modulus and shear modulus.

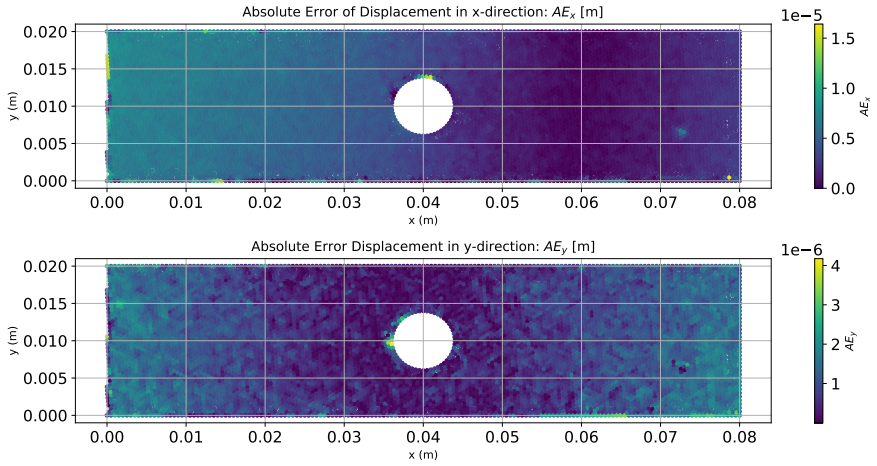

Figure 4: Absolute error between the displacement from the calibrated FEM simulation and Experimental data

References

Ulrich Römer, Stefan Hartmann, Jendrik-Alexander Tröger, David Anton, Henning Wessels, Moritz Flaschel, and Laura De Lorenzis. Reduced and all-at-once approaches for model calibration and discovery in computational solid mechanics. *Applied Mechanics Reviews*, pages 1–51, 2024.

David Anton and Henning Wessels. Physics-informed neural networks for material model calibration from full-field displacement data. *arXiv preprint arXiv:2212.07723*, 2022.

David Anton, Jendrik-Alexander Tröger, Henning Wessels, Ulrich Römer, Alexander Henkes, and Stefan Hartmann. Deterministic and statistical calibration of constitutive models from full-field data with parametric physics-informed neural networks. *arXiv preprint arXiv:2405.18311*, 2024.

Lennart Paul, Jorge-Humberto Urrea-Quintero, Umer Fiaz, Ali Hussein, Hazem Yaghi, Henning Wessels, Ulrich Römer, and Joachim Stahlmann. Gaussian processes enabled model calibration in the context of deep geological disposal. *arXiv preprint arXiv:2409.02576*, 2024.

Gopal Agarwal, Jorge-Humberto Urrea-Quintero, Henning Wessels, and Thomas Wick. Parameter identification and uncertainty propagation of hydrogel coupled diffusion-deformation using pod-based reduced-order modeling. *Computational Mechanics*, pages 1–31, 2024.

Igor A. Baratta, Joseph P. Dean, Jørgen S. Dokken, Michal Habera, Jack S. Hale, Chris N. Richardson, Marie E. Rognes, Matthew W. Scroggs, Nathan Sime, and Garth N. Wells. Dolfinx: The next generation fenics problem solving environment. *Zenodo*, 2023. doi: 10.5281/zenodo.10447666. URL `https://zenodo.org/records/10447666`.

J.-A. Tröger, S. Hartmann, D. Anton, and H. Wessels. Digital image correlation measurement of linear elastic steel specimen, 2024. URL `https://doi.org/10.5281/zenodo.11257192`.